

# Constraints on $\Xi^-$ nuclear interactions from capture events in emulsion

E. Friedman, A. Gal\*

*Racah Institute of Physics, The Hebrew University, Jerusalem 91904, Israel*

---

## Abstract

Five  $\Xi^-p \rightarrow \Lambda\Lambda$  two-body capture events in  $^{12}\text{C}$  and  $^{14}\text{N}$  emulsion nuclei, in which a pair of single- $\Lambda$  hypernuclei is formed and identified by their weak decay, have been observed in  $(K^-, K^+)$  emulsion exposures at KEK and J-PARC. Applying a  $\Xi^-$ -nucleus optical potential methodology to study atomic and nuclear transitions, we confirm that these capture events occur from Coulomb assisted  $1p_{\Xi^-}$  nuclear states. Long-range  $\Xi N$  shell-model correlations are found essential to achieve consistency between the  $^{12}\text{C}$  and  $^{14}\text{N}$  events. The resulting  $\Xi$ -nuclear interaction is strongly attractive, with  $\Xi$  potential depth in nuclear matter  $V_{\Xi} \gtrsim 20$  MeV. Implications to multi-strangeness features of dense matter are outlined.

*Keywords:* hyperon strong interactions;  $\Xi^-$  atoms and hypernuclei.

---

## 1. Introduction and background

Recent two-particle correlation studies of  $p\Lambda$ ,  $\Lambda\Lambda$  and  $\Xi^-p$  pairs measured by ALICE [1, 2, 3, 4] in  $pp$  and  $p\text{-Pb}$  ultra-relativistic collisions at TeV energies have triggered renewed interest in Strangeness  $\mathcal{S} \neq 0$  baryon-baryon interactions and consequences thereof to strange hadronic matter. In particular, the  $\Xi^-p$  interaction was shown to be attractive [3], in good agreement with the recent HAL-QCD lattice calculations reaching  $m_{\pi} = 146$  MeV [5]. Understanding the strength of the  $\mathcal{S} = -2$   $\Xi N$  interaction, particularly when embedded in nuclear media, is vital for resolving the Hyperon Puzzle which addresses the fate of hyperons in dense neutron-star matter [6].

---

\*corresponding author: Avraham Gal, avragal@savion.huji.ac.il

Little is known from experiment on the nuclear interaction of  $\Xi$  hyperons [7, 8]. A standard reaction production is the nuclear  $(K^-, K^+)$  reaction, driven by  $K^-p \rightarrow K^+\Xi^-$  strangeness exchange on protons. Owing to its large momentum transfer, the produced  $\Xi^-$  hyperons populate dominantly the quasi-free continuum region, with less than 1% expected to populate  $\Xi^-$ -nuclear bound states that decay subsequently by the  $\Xi^-p \rightarrow \Lambda\Lambda$  strong-interaction capture reaction. Analysis of old emulsion events attributed to the formation of  $\Xi$  hypernuclei suggested attractive Woods-Saxon  $\Xi$  nuclear potential depth  $V_\Xi=21\text{-}24$  MeV [9]. While this range of values is considered sufficient for  $\Xi$  hyperons to play an active role in strange hadronic matter [10] and in neutron stars [11], somewhat smaller values follow from studies of dedicated  $(K^-, K^+)$  counter experiments:  $V_\Xi \lesssim 20$  MeV in KEK PS-E224 [12],  $V_\Xi \sim 14$  MeV in BNL AGS-E885 [13], both on  $^{12}\text{C}$ , and  $V_\Xi = 17 \pm 6$  MeV on  $^9\text{Be}$  [14] from BNL AGS-E906 [15]. New results from the J-PARC E05 and E70  $(K^-, K^+)$  experiments on  $^{12}\text{C}$  are forthcoming [16]. However, no  $\Xi^-$  or  $\Lambda\Lambda$  hypernuclear bound states have ever been observed unambiguously in these experiments. Powerful future experiments by the PANDA Collaboration at FAIR [17], using  $\bar{p}p \rightarrow \Xi^-\bar{\Xi}^+$  or  $\bar{p}n \rightarrow \Xi^-\bar{\Xi}^0$  production modes, and also at BESIII [18] focusing on the  $J/\psi \rightarrow \Xi^-\bar{\Xi}^+ O(10^{-3})$  decay branch, are likely to change this state of the art.

The situation is different in exposures of light-emulsion CNO nuclei to the  $(K^-, K^+)$  reaction, in which a tiny fraction of the produced high-energy  $\Xi^-$  hyperons slow down in the emulsion, undergoing an Auger process to form high- $n$  atomic levels, and cascade down radiatively. Cascade essentially terminates, when strong-interaction capture takes over, in a 3D atomic state bound by 126, 175, 231 keV in C, N, O, respectively. The 3D strong-interaction shift is less than 1 keV [19]. Capture events are recorded by observing  $\Lambda$  hyperon or hypernuclear decay products. Interestingly, whereas the few observed double- $\Lambda$  hypernucleus production events are consistent with  $\Xi^-$  capture from atomic 3D states [8], formation of pairs of single- $\Lambda$  hypernuclei requires capture from a lower  $\Xi^-$  orbit. Expecting the final two  $\Lambda$  hyperons in  $\Xi^-p \rightarrow \Lambda\Lambda$  capture to be formed in a  $S=0, 1s_\Lambda^2$  configuration, the initial  $\Xi^-$  hyperon and the proton on which it is captured must satisfy  $l_{\Xi^-} = l_p$  [20] which for  $p$ -shell nuclear targets favors the choice  $l_{\Xi^-} = 1$ . Indeed, all two-body  $\Xi^-$  capture events,  $\Xi^- + {}^AZ \rightarrow {}^{A'}_\Lambda Z' + {}^{A''}_\Lambda Z''$ , to twin single- $\Lambda$  hypernuclei reported from KEK and J-PARC light-emulsion  $K^-$  exposures [21, 22, 23], as listed here in Table 1, are consistent with  $\Xi^-$  capture from Coulomb-assisted  $1p_{\Xi^-}$  nuclear states bound by  $\sim 1$  MeV.

Table 1: Reported two-body  $\Xi^-$  capture events  $\Xi^- + {}^A Z \rightarrow {}^A{}'_\Lambda Z' + {}^A{}''_\Lambda Z''$  in light-emulsion nuclei to a pair of single- $\Lambda$  hypernuclei, some in ground states, some in specific excited states marked by asterisk. Only the first and last events are uniquely assigned. Fitted  $\Xi^-$  binding energies  $B_{\Xi^-}$  are listed.

Experiment	Event	${}^A Z$	${}^A{}'_\Lambda Z' + {}^A{}''_\Lambda Z''$	$B_{\Xi^-}$ (MeV)
KEK E176 [21]	10-09-06	${}^{12}\text{C}$	${}^4_\Lambda\text{H} + {}^9_\Lambda\text{Be}$	$0.82 \pm 0.17$
KEK E176 [21]	13-11-14	${}^{12}\text{C}$	${}^4_\Lambda\text{H} + {}^9_\Lambda\text{Be}^*$	$0.82 \pm 0.14$
KEK E176 [21]	14-03-35	${}^{14}\text{N}$	${}^3_\Lambda\text{H} + {}^{12}_\Lambda\text{B}$	$1.18 \pm 0.22$
KEK E373 [22]	KISO	${}^{14}\text{N}$	${}^5_\Lambda\text{He} + {}^{10}_\Lambda\text{Be}^*$	$1.03 \pm 0.18$
J-PARC E07 [23]	IBUKI	${}^{14}\text{N}$	${}^5_\Lambda\text{He} + {}^{10}_\Lambda\text{Be}$	$1.27 \pm 0.21$

In Table 1 only the first and last listed events are uniquely assigned in terms of initial emulsion nucleus  ${}^A Z$  and final single- $\Lambda$  hypernuclei  ${}^A{}'_\Lambda Z' + {}^A{}''_\Lambda Z''$  ground states, providing thereby a unique value of  $B_{\Xi^-}$  per each event. The events fitted by assuming specific excited states  ${}^A{}''_\Lambda Z''^*$  are equally well fitted each by g.s. assignments  ${}^A{}''_\Lambda Z''$ , with values of  $B_{\Xi^-}$  as high as  $\sim 4$  MeV, and the middle event is equally well fitted as a capture event in  ${}^{16}\text{O}$ , to  ${}^3_\Lambda\text{H} + {}^{14}_\Lambda\text{C}$  with  $B_{\Xi^-} = 0.46 \pm 0.39$  MeV or to  ${}^4_\Lambda\text{H} + {}^{13}_\Lambda\text{C}$  with  $B_{\Xi^-} = 0.40 \pm 0.27$  MeV, both consistent with  $\Xi^-$  capture from an atomic 3D state. We note that the listed  $\Xi^-$  binding energy  $B_{\Xi^-}$  values are all around 1 MeV, significantly higher than the purely-Coulomb atomic 2P binding energy values which are approximately 0.3, 0.4, 0.5 MeV in C,N,O atoms, respectively. These  $\sim 1$  MeV  $B_{\Xi^-}$  values correspond to  $1p_{\Xi^-}$  nuclear states that evolve from 2P atomic states upon adding a strong-interaction  $\Xi$  nuclear potential.<sup>1</sup> This interpretation is the only one common to *all* five events.

Not listed in the table are multi-body capture events that require for their interpretation undetected capture products, usually neutrons, on top of a pair of single- $\Lambda$  hypernuclei. Most of these new J-PARC E07 events [24] imply  $\Xi^-$  capture from  $1s_{\Xi^-}$  nuclear states, with capture rates  $\mathcal{O}(10^{-2})$  of capture rates from the  $1p_{\Xi^-}$  nuclear states considered here [20, 25].

In the present work we consider  $\Xi^-$  atomic and nuclear transitions in light emulsion atoms, first with a  $t\rho$  optical potential, to substantiate that

<sup>1</sup>Nuclear single-particle (s.p.) states are denoted by lower-case letters:  $1s, 1p, 1d, \dots$  for the lowest  $l$  values, in distinction from atomic s.p. states denoted by capitals:  $1S, 2P, 3D, \dots$  for the lowest  $L$  values.

$\Xi^- p \rightarrow \Lambda\Lambda$  capture indeed occurs from a Coulomb-assisted nuclear  $1p_{\Xi^-}$  state in light emulsion nuclei. The strength of this  $\Xi$ -nuclear potential is determined by requiring that it reproduces a  $1p_{\Xi^-}$  state in  $^{12}\text{C}(0_{\text{g.s.}}^+)$  bound by  $0.82 \pm 0.15$  MeV from Table 1. Disregarding temporarily the  $s_{\Xi^-} = \frac{1}{2}$  Pauli-spin degree of freedom, we proceed to discuss the implications of identifying the value  $B_{\Xi^-} \approx 1.15 \pm 0.20$  MeV for  $^{14}\text{N}$  from Table 1 with the binding energy of  $\mathcal{L}^\pi = (0^-, 1^-, 2^-)$  triplet of  $1p_{\Xi^-}$  nuclear states built on  $J^\pi(^{14}\text{N}_{\text{g.s.}}) = 1^+$ , thereby linking the capture process to properties of the  $\Xi$ -nucleus residual interaction. This provides the only self consistent deduction of the  $\Xi$ -nuclear interaction strength from analysis of the five  $\Xi^-$  capture events in light nuclear emulsion, fitted to two-body formation of specific  $\Lambda$  hypernuclei, as listed in Table 1. The resulting  $t\rho$   $\Xi$  potential depth at nuclear-matter density  $\rho_0 = 0.17 \text{ fm}^{-3}$  is  $V_{\Xi} \approx 24$  MeV. We then improve upon the  $t\rho$  leading term of the optical potential by introducing the next, Pauli correlation term in the optical potential density expansion [26]. This leads to  $\approx 10\%$  reduction of  $V_{\Xi}$ , down to  $V_{\Xi} \approx 22$  MeV, keeping it within the optical potential approach well above 20 MeV. Our results suggest that  $1s_{\Xi^-}$  nuclear bound states exist all the way down to  $^4\text{He}$ , with potentially far-reaching implications for the role of  $\Xi$  hyperons in multi-strange dense matter.

A value  $V_{\Xi} \gtrsim 20$  MeV implies a substantially stronger in-medium  $\Xi N$  attraction than reported by some recent model evaluations (HAL-QCD [27], EFT@NLO [28, 29], RMF [30]) all of which satisfy  $V_{\Xi} \lesssim 10$  MeV. A notable exception is provided by versions ESC16\*(A,B) of the latest Nijmegen extended-soft-core  $\Xi N$  interaction model [31], in which values of  $V_{\Xi}$  higher than 20 MeV are derived. However, these large values are reduced substantially by  $\Xi NN$  three-body contributions within the same ESC16\* model.

## 2. Methodology

The starting point in optical-potential analyses of hadronic atoms [32] is the in-medium hadron self-energy  $\Pi(E, \vec{p}, \rho)$  that enters the in-medium hadron (here  $\Xi$  hyperon) dispersion relation

$$E^2 - \vec{p}^2 - m_{\Xi}^2 - \Pi(E, \vec{p}, \rho) = 0, \quad (1)$$

where  $\vec{p}$  and  $E$  are the  $\Xi$  momentum and energy, respectively, in nuclear matter of density  $\rho$ . The resulting  $\Xi$ -nuclear optical potential  $V_{\text{opt}}$ , defined by  $\Pi(E, \vec{p}, \rho) = 2EV_{\text{opt}}$ , enters the near-threshold  $\Xi^-$  wave equation

$$[\nabla^2 - 2\mu(B + V_{\text{opt}} + V_c) + (V_c + B)^2] \psi = 0, \quad (2)$$

where  $\hbar = c = 1$ . Here  $\mu$  is the  $\Xi^-$ -nucleus reduced mass,  $B$  is the complex binding energy,  $V_c$  is the finite-size Coulomb potential of the  $\Xi^-$  hyperon with the nucleus, including vacuum-polarization terms, all added according to the minimal substitution principle  $E \rightarrow E - V_c$ . Strong-interaction optical-potential  $V_{\text{opt}}$  terms other than  $2\mu V_{\text{opt}}$  are negligible and omitted here. The use of a Klein-Gordon wave equation (2) for the  $\Xi^-$  fermion rather than Dirac equation provides an excellent approximation when  $Z\alpha \ll 1$  and fine-structure effects are averaged on, as for the X-ray transitions considered here.  $\Xi^-$  nuclear spin-orbit effects are briefly mentioned below.

For  $V_{\text{opt}}$  in Eq. (2) we first use a standard  $t\rho$  form [32]

$$V_{\text{opt}}(r) = -\frac{2\pi}{\mu} \left(1 + \frac{A-1}{A} \frac{\mu}{m_N}\right) [b_0 \rho(r) + b_1 \rho_{\text{exc}}(r)], \quad (3)$$

where the complex strength parameters  $b_0$  and  $b_1$  are effective, generally density dependent  $\Xi N$  isoscalar and isovector c.m. scattering amplitudes respectively. The density  $\rho = \rho_n + \rho_p$  is a nuclear density distribution normalized to the number of nucleons  $A$  and  $\rho_{\text{exc}} = \rho_n - \rho_p$  is a neutron-excess density with  $\rho_n = (N/Z)\rho_p$ , implying that  $\rho_{\text{exc}} = 0$  for the  $N = Z$  emulsion nuclei  $^{12}\text{C}$  and  $^{14}\text{N}$  analyzed in the next section. Here we used mostly nuclear density distributions of harmonic-oscillator (HO) type [33] where the r.m.s. radius of  $\rho_p$  was set equal to that of the known nuclear charge density [34]. Folding reasonably chosen  $\Xi N$  interaction ranges other than corresponding to the proton charge radius, or using Modified Harmonic Oscillator (MHO) densities, or replacing HO densities by realistic three-parameter Fermi (3pF) density distributions [35, 36] made little difference: all the calculated binding energies changed by a small fraction, about 0.03 MeV of the uncertainty imposed by the  $\pm 0.15$  MeV experimental uncertainty of the 0.82 MeV  $1p_{\Xi}$  binding energy in  $^{12}\text{C}$  listed in Table 1. We note that the central density  $\rho(0)$  in all density versions used here is within acceptable values for nuclear matter, i.e., between roughly 0.15 and 0.20  $\text{fm}^{-3}$ .

The form of  $V_{\text{opt}}$  given by Eq. (3) corresponds to a central-field approximation of the  $\Xi$ -nuclear interaction. Spin and isospin degrees of freedom induced by the most general two-body  $s$ -wave  $\Xi N$  interaction  $V_{\Xi N}$ ,

$$V_{\Xi N} = V_0 + V_\sigma \sigma_{\Xi} \cdot \sigma_N + V_\tau \tau_{\Xi} \cdot \tau_N + V_{\sigma\tau} \sigma_{\Xi} \cdot \sigma_N \tau_{\Xi} \cdot \tau_N \quad (4)$$

with  $V$ s functions of  $r_{\Xi N}$ , are suppressed in this approach. Choosing  $^{12}\text{C}_{\text{g.s.}}$  with isospin  $I = 0$  and spin-parity  $J^\pi = 0^+$  for a nuclear medium offers

the advantage that only  $V_0$  is operative in leading order since the nuclear expectation value of each of the other three terms in Eq. (4) vanishes. But for  $^{14}\text{N}_{\text{g.s.}}$ , with  $I(J^\pi)=0(1^+)$ ,  $V_\sigma$  is operative as well, adding unavoidable model dependence of order  $\mathcal{O}(1/A)$  to  $\Xi^-$ -nuclear potential depth values derived from capture events assigned to this emulsion nucleus. For this reason we start the present analysis with the two  $\Xi^-$ - $^{12}\text{C}$  emulsion events of Table 1.

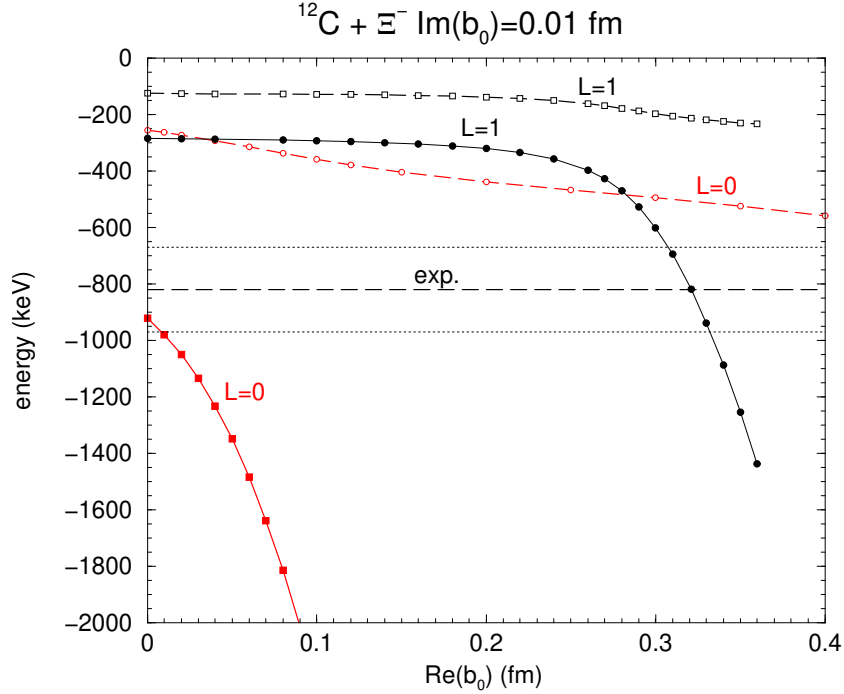


Figure 1: Energy levels (in keV) of the lowest  $\Xi^-$  atomic states for  $L=0$  (1S,2S) and  $L=1$  (2P,3P) in  $^{12}\text{C}$  as a function of the strength parameter  $\text{Re } b_0$  (in fm) of the  $\Xi^-$  optical potential (3). Spin-orbit splittings of  $L=1$  states are suppressed in this figure. The dashed and dotted horizontal lines mark the value  $B_{\Xi^-} = 0.82 \pm 0.15$  MeV from Table 1.

### 3. $\Xi^-$ capture in $^{12}\text{C}$

Figure 1 shows a portion of the combined atomic plus nuclear spectrum of  $\Xi^-$  in  $^{12}\text{C}$ ,  $B_{\Xi^-} \leq 2$  MeV, as a function of  $\text{Re } b_0$ , Eq. (3), for a fixed  $\text{Im } b_0 = 0.01$  fm corresponding to a nuclear-matter  $\Xi^-$  capture width  $\Gamma_{\Xi^-} \approx 1.5$  MeV, compatible with the HAL-QCD weak  $\Xi^- p \rightarrow \Lambda\Lambda$  transition

potential [5]. Plotted are the energies of the two lowest states of each orbital angular momentum  $l_{\Xi^-} = 0, 1$ , starting at  $\text{Re } b_0 = 0$  with almost purely atomic states 1S, 2P, 2S, 3P from bottom up. Of these states the 1S state with Bohr radius about 3.8 fm is indistinguishable from a nuclear 1s state, and indeed it dives down in energy as soon as  $\text{Re } b_0$  is made nonzero. It takes considerable strength,  $\text{Re } b_0 \gtrsim 0.25$  fm, before the next atomic state, 2P with Bohr radius about 15 fm, overlaps appreciably with the  $^{12}\text{C}_{\text{g.s.}}$  nuclear core, diving down in energy to become a nuclear  $1p$  state. The higher two states that start as atomic 2S, 3P remain largely atomic as  $\text{Re } b_0$  is varied in Fig. 1. Their slowly decreasing energies indicate a rearrangement of the atomic spectrum [37]:  $2\text{S} \rightarrow 1\text{S}$  and  $3\text{P} \rightarrow 2\text{P}$ . Judging by the marked band of values  $B_{\Xi^-} = 0.82 \pm 0.15$  MeV for the two KEK E176 events listed in Table 1, the figure suggests that they are compatible with a  $1p_{\Xi^-}$  nuclear state corresponding to a  $\Xi$ -nuclear potential strength of  $\text{Re } b_0 = 0.32 \pm 0.01$  fm. The sensitivity to variations of  $\text{Im } b_0$  is minimal: choosing  $\text{Im } b_0 = 0.04$  fm [19] instead of 0.01 fm increases  $\text{Re } b_0$  by 0.01 fm to  $0.33 \pm 0.01$  fm.

Radiative rates for E1 transitions from the  $\Xi^-$  atomic 3D state to the  $\Xi^-$  atomic 3P state, and to the  $1p_{\Xi^-}$  nuclear state that started as atomic 2P state are found comparable to each other, accounting together for 7.6% of the total 3D width  $\Gamma_{3\text{D}} = 3.93$  eV as obtained using the optical potential (3). However, the subsequent  $\Xi^- p \rightarrow \Lambda\Lambda$  capture will proceed preferentially from the  $1p_{\Xi^-}$  nuclear state that offers good overlap between the  $1p_{\Xi^-}$  and  $1p_p$  valence-proton orbits. Since the final  $1s_{\Lambda}^2$  configuration has  $J_f = 0$ , and the  $p$ -shell protons in  $^{12}\text{C}$  are mostly in  $j = \frac{3}{2}$  orbits, the requirement  $J_i = J_f = 0$  imposes  $j_{\Xi^-} = \frac{3}{2}$  on the spin-orbit doublet members of the  $1p_{\Xi^-}$  state. The shift of this  $1p_{\Xi^-}(\frac{3}{2})$  sub level from the  $1p_{\Xi^-}$   $(2j+1)$ -average is estimated, based on the 152 keV  $1p_{\Lambda}$  spin-orbit splitting observed in  $^{13}_{\Lambda}\text{C}$  [38] to be less than 100 keV upward [39] and, hence, within the 0.15 MeV listed uncertainty introduced here for the position of the  $(2j+1)$ -averaged  $1p_{\Xi^-}$  state.

#### 4. Spectroscopy of $^{14}\text{N}_{\text{g.s.}} + 1p_{\Xi^-}$ states

Having derived the strength parameter  $\text{Re } b_0 = 0.32 \pm 0.01$  fm of  $V_{\text{opt}}$  by fitting it to  $B_{\Xi^-}^{1p}(^{12}\text{C}) = 0.82 \pm 0.15$  MeV, we apply this optical potential to  $^{14}\text{N}$  where it yields  $B_{\Xi^-}^{1p}(^{14}\text{N}) = 2.08 \pm 0.28$  MeV, considerably higher than the value  $B_{\Xi^-} = 1.15 \pm 0.20$  MeV obtained from the three events assigned in Table 1 to  $\Xi^-$  capture in  $^{14}\text{N}$ . However, this calculated  $B_{\Xi^-}^{1p}(^{14}\text{N})$  corresponds to a  $(2\mathcal{L} + 1)$ -average of binding energies for a triplet of states  $\mathcal{L}^{\pi} = (0^-, 1^-, 2^-)$

obtained by coupling a  $1p_{\Xi^-}$  state to  $J^\pi(^{14}\text{N}_{\text{g.s.}})=1^+$ , as shown in Fig. 2. We now discuss the splitting of these triplet states. Effects of  $\Xi^-$  Pauli spin,  $s_{\Xi^-} = \frac{1}{2}$ , are introduced at a later stage.

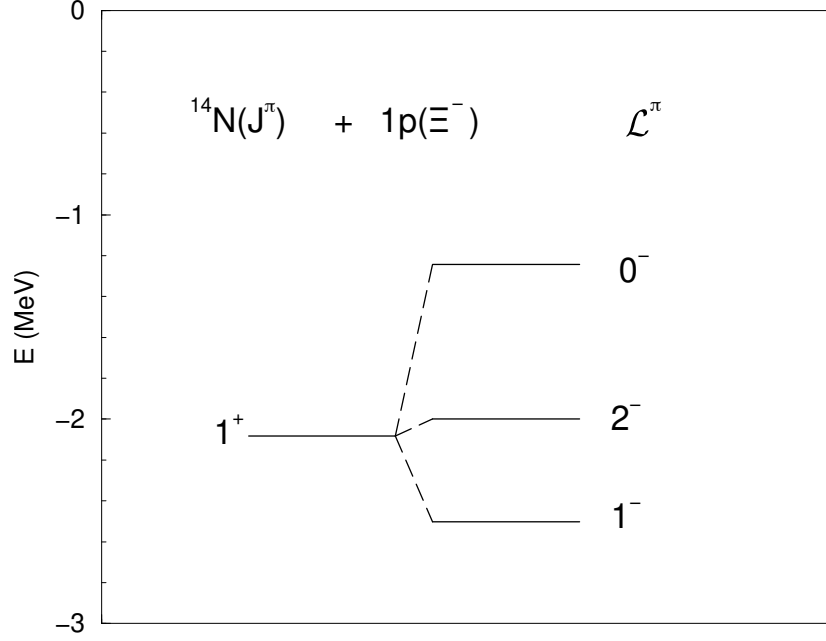


Figure 2: Energies (in MeV) of  $\mathcal{L}^\pi = (0^-, 1^-, 2^-)$  triplet of  $^{14}\text{N}_{\text{g.s.}} + 1p_{\Xi^-}$  states, split by a  $Q_N \cdot Q_{\Xi}$  residual interaction (5). The  $(2\mathcal{L} + 1)$ -averaged energy  $-2.08 \pm 0.28$  MeV was calculated using the same optical potential parameter  $b_0$  that yields a  $^{12}\text{C}_{\text{g.s.}} + 1p_{\Xi^-}$  state at  $-0.82 \pm 0.15$  MeV, corresponding to the  $\Xi^-$  capture events in  $^{12}\text{C}$  listed in Table 1.

The construction of the  $^{14}\text{N}_{\text{g.s.}} + 1p_{\Xi^-}$  spectrum in Fig. 2 follows a similar  $^{12}\text{C}(2^+; 4.44 \text{ MeV}) + 1p_{\Lambda}$  spectrum construction in  $^{13}_{\Lambda}\text{C}$  [40]. The energy splittings marked in the figure are obtained from a two-body spin-independent interaction  $V_0(r_{\Xi N})$ , Eq. (4), between a  $p$ -shell  $\Xi$  hyperon and  $p$ -shell nucleons, expressed in terms of its shell-model (SM) quadrupole-quadrupole residual interaction  $\mathcal{V}_{\Xi N}$ ,

$$\mathcal{V}_{\Xi N} = F_{\Xi N}^{(2)} Q_N \cdot Q_{\Xi}, \quad Q_B = \sqrt{\frac{4\pi}{5}} Y_2(\hat{r}_B), \quad (5)$$

where  $F^{(2)}$  is the corresponding Slater integral [41]. A representative value of  $F_{\Xi N}^{(2)} = -3$  MeV is used here, smaller than the value  $F_{\Lambda N}^{(2)} = -3.7$  MeV



established empirically for  $p$ -shell  $\Lambda$  hypernuclei [42], in accordance with a  $\Xi N$  strong interaction somewhat weaker than the  $\Lambda N$  strong interaction (see next section). A single  ${}^3D_1$   ${}^{14}\text{N}_{\text{g.s.}}$  SM component providing a good approximation to the full SM intermediate-coupling g.s. wavefunction [43] was assumed in the present evaluation.

Fig. 2 exhibits a triplet of  ${}^{14}\text{N}_{\text{g.s.}} + 1p_{\Xi^-}$  levels, spread over more than 1 MeV. The least bound triplet state, with  $\mathcal{L}^\pi = 0^-$ , is shifted upward by 0.84 MeV from the  $(2\mathcal{L} + 1)$  averaged position at  $-2.08 \pm 0.28$  MeV to  $E(0^-) = -1.24 \pm 0.28$  MeV. This is consistent with the averaged position  $\bar{E} = -1.15 \pm 0.20$  MeV of the three  $\Xi^-$   ${}^{14}\text{N}_{\text{g.s.}}$  capture events listed in Table 1. We are not aware of any good reason why capture has not been seen from the other two states with  $\mathcal{L}^\pi = 1^-, 2^-$ . This may change when more events are collected at the next stage of the ongoing J-PARC E07 emulsion experiment.

Table 2: Quadrupole-quadrupole contributions to the energies  $E(\mathcal{L}^\pi)$  of the  ${}^{14}\text{N}_{\text{g.s.}} + 1p_{\Xi^-}$  triplet of states shown in Fig. 2 with respect to  $E({}^{14}\text{N}_{\text{g.s.}})$ , using  $F_{\Xi N}^{(2)} = -3$  MeV, and spin contributions to the splittings  $\Delta E(\mathcal{L}) = E(J = \mathcal{L} + \frac{1}{2}) - E(J = \mathcal{L} - \frac{1}{2})$  of the  $\mathcal{L} \neq 0$  states.  $A_{ls}$  and  $A_{ss}$  are spin-orbit ( $l_\Xi = 1, s_\Xi = \frac{1}{2}$ ) and spin-spin ( $s_N = s_\Xi = \frac{1}{2}$ ) energy splittings, respectively, see text.

Interaction	$E(0^-)$	$E(1^-)$	$E(2^-)$	$\Delta E(1^-)$	$\Delta E(2^-)$
$Q_N \cdot Q_\Xi$	$-\frac{7}{25} F_{\Xi N}^{(2)}$	$\frac{7}{50} F_{\Xi N}^{(2)}$	$-\frac{7}{250} F_{\Xi N}^{(2)}$	—	—
$l_\Xi \cdot s_\Xi$	—	—	—	$\frac{1}{2} A_{ls}$	$\frac{5}{6} A_{ls}$
$s_N \cdot s_\Xi$	—	—	—	$\frac{3}{8} A_{ss}$	$\frac{5}{8} A_{ss}$

Introducing Pauli spin,  $s_{\Xi^-} = \frac{1}{2}$ , the total angular momentum of the uppermost level marked  $0^-$  in Fig. 2 becomes  $J^\pi = \frac{1}{2}^-$ , but its position is unaffected by spin-orbit and spin-spin interactions. Each of the other two levels in Fig. 2 splits into a doublet  $J = \mathcal{L} \pm \frac{1}{2}$  whose  $(2J + 1)$ -average remains in the unsplit position. Estimated splittings are listed in Table 2 in terms of two constituent spin matrix elements:  $A_{ls} \lesssim 300$  keV [39] for the  $l_\Xi \cdot s_\Xi$  spin-orbit splitting  $E_{1p_\Xi}(\frac{3}{2}^-) - E_{1p_\Xi}(\frac{1}{2}^-)$ , and  $A_{ss} \approx 400 \pm 80$  keV for the  $s_N \cdot s_\Xi$  spin-spin splitting  $E(S_{\Xi N} = 0) - E(S_{\Xi N} = 1)$  for  $p$ -shell nucleon and  $\Xi$  hyperon. For estimating  $A_{ss}$  we used the HAL-QCD [5] volume integral of  $V_\sigma$ , Eq. (4), relative to that of  $V_0$ , thereby generating about 20% systematic uncertainty. Incorporating these spin splittings into the  $\mathcal{L}^\pi = (0^-, 1^-, 2^-)$  triplet in Fig. 2 keeps the  $\mathcal{L}^\pi = 0^-$  state of interest, which has become  $J^\pi = \frac{1}{2}^-$ , well separated by at least 0.5 MeV from the rest of the split states.

## 5. Density dependence, $\Xi$ nuclear potential depth and $1s_{\Xi^-}$ states

So far we have discussed a density independent  $t$ -matrix element  $b_0$  in  $V_{\text{opt}}$ , Eq. (3), to fit the  $\Xi^-$  capture events in  $^{12}\text{C}$  from Table 1. The resulting value  $\text{Re } b_0 = 0.32 \pm 0.01$  fm implies, in the limit  $A \rightarrow \infty$  and  $\rho(r) \rightarrow \rho_0 = 0.17 \text{ fm}^{-3}$ , a value  $V_{\Xi} = 24.3 \pm 0.8$  MeV in nuclear matter, in accordance with the extraction of  $V_{\Xi}$  from old emulsion events [9] but exceeding considerably other values reviewed in the Introduction. To explore how robust this conclusion is, we introduce the next to leading-order density dependence of  $V_{\text{opt}}$ , replacing  $\text{Re } b_k$  ( $k=0,1$ ) in Eq. (3) by

$$\text{Re } b_k(\rho) = \frac{\text{Re } b_k}{1 + \frac{3k_F}{2\pi} \text{Re } b_0^{\text{lab}}}, \quad k_F = (3\pi^2 \rho/2)^{\frac{1}{3}}, \quad (6)$$

where  $k_F$  is the Fermi momentum corresponding to nuclear density  $\rho$  and  $b_0^{\text{lab}} = (1 + \frac{m_{\Xi^-}}{m_N})b_0$  is the lab transformed form of the c.m. scattering amplitude  $b_0$ . Eq. (6) accounts for Pauli exclusion correlations in  $\Xi N$  in-medium multiple scatterings [26, 44]. Variants of the form (6) have been used in kaonic atoms [45] and mesic nuclei [46, 47, 48] calculations. Shorter-range correlations, disregarded here, were shown in Ref. [46] to contribute less than  $\sim 30\%$  of the long-range Pauli correlation term. Applying Eq. (6) in the present context,  $B_{\Xi^-}^{1p}(^{12}\text{C}) = 0.82$  MeV is refitted by  $\text{Re } b_0 = 0.527$  fm, lowering the former value  $B_{\Xi^-}^{1p}(^{14}\text{N}) = 2.08$  MeV to 1.95 MeV without any substantive change in the conclusions drawn above regarding the five two-body capture events deciphered here. The nuclear-matter  $\Xi$ -nuclear potential depth  $V_{\Xi}$  decreases from  $24.3 \pm 0.8$  to  $21.9 \pm 0.7$  MeV, a decrease of merely 10%, with additional systematic uncertainty of less than 1 MeV. This value of  $V_{\Xi}$  is sufficient to bind  $1s_{\Xi^-}$  states in  $p$ -shell nuclei, with systematic uncertainty of less than 0.5 MeV, as demonstrated in Table 3 which shows a steady decrease of  $B_{\Xi^-}^{1s}$  and  $\Gamma_{\Xi^-}^{1s}$  down to  $^4\text{He}$ . The increased  $\Gamma_{\Xi^-}^{1s}(^4\text{He})$  reflects a denser  $^4\text{He}$  medium. However, expecting corrections of order  $\mathcal{O}(1/A)$  to the optical potential methodology, our  $^4\text{He}$  result should be taken with a grain of salt. It is worth noting that all listed  $1s_{\Xi^-}$  g.s. levels remain bound also when the attractive finite-size Coulomb interaction  $V_c$  is switched off. None of such  $1s_{\Xi^-}$  states have been observed conclusively in dedicated experiments.

The  $T = \frac{1}{2}$   $^{11}\text{B}$  nucleus, the only  $T \neq 0$  nucleus listed in Table 3, requires in addition to the isoscalar parameter  $b_0 = 0.527 + i0.010$  fm also a knowledge of the isovector parameter  $b_1$ . Here we used the HAL-QCD [5] volume integral of  $V_{\tau}(r_{\Xi N})$  relative to that of  $V_0(r_{\Xi N})$ , Eq. (4), to estimate  $b_1$  relative to

Table 3: Binding energies  $B_{\Xi^-}^{1s}$  and widths  $\Gamma_{\Xi^-}^{1s}$  (in MeV) in core nuclei  ${}^AZ(J_c)$ , g.s. spin  $J_c$ , obtained by solving Eq. (2) with  $b_0 = 0.527 + i0.010$  fm and  $b_1 = -0.225$  fm in  $V_{\text{opt}}$ , Eqs. (3),(6). A finite-size Coulomb interaction  $V_c$  is included.

	${}^{14}\text{N}(1)$	${}^{12}\text{C}(0)$	${}^{11}\text{B}(\frac{3}{2})$	${}^{10}\text{B}(3)$	${}^6\text{Li}(1)$	${}^4\text{He}(0)$
$B_{\Xi^-}^{1s}$	11.5	9.8	8.4	7.6	2.1	2.0
$\Gamma_{\Xi^-}^{1s}$	1.02	0.93	0.89	0.77	0.26	0.45

$b_0$ , thereby deriving a value  $b_1 = -0.225$  fm.<sup>2</sup> The resulting value  $B_{\Xi^-}^{1s}({}^{11}\text{B})$  listed in the table is lower by 530 keV than obtained disregarding  $b_1$ . Next, we introduce  $s_{\Xi^-} = \frac{1}{2}$  Pauli spin, splitting each of the listed  $1s_{\Xi^-}$  levels in  $J_c \neq 0$  core nuclei into two sub levels  $J = J_c \pm \frac{1}{2}$ . Using HAL-QCD [5] ratios of volume integrals of  $V_\sigma(r_{\Xi N})$  and  $V_{\sigma\tau}(r_{\Xi N})$  to that of  $V_0(r_{\Xi N})$ , Eq. (4), as done above for  $V_\tau$ , we estimate the  $1s_{\Xi^-}$  spin splittings to be well below 1 MeV. Other potential sources of  $\Xi^-$  spin splittings that are relevant in  $\Lambda$  hypernuclei, such as tensor or induced nuclear spin-orbit terms, are likely to be considerably weaker than evaluated in Ref. [49] and are disregarded here. Of particular interest is the  $({}^{11}\text{B}_{\text{g.s.}} + 1s_{\Xi^-})$   $J^\pi = 1^-$  doublet member expected to be formed in the  ${}^{12}\text{C}(K^-, K^+)$  production reaction when the outgoing  $K^+$  meson is detected in the forward direction. Our estimates place it about 0.5 MeV deeper than the listed  $(2J+1)$ -averaged  $B_{\Xi^-}^{1s}({}^{11}\text{B})=8.4$  MeV, contrasting statements, e.g. [8], that adopt  $B_{\Xi^-}^{1s}({}^{11}\text{B})\sim 5$  MeV from the BNL AGS-E885  ${}^{12}\text{C}(K^-, K^+)$  experiment [13]. In fact, the E885 poor resolution prevents making any such conclusive statement.

## 6. Conclusion

We have shown that all five light nuclear emulsion events identified in KEK and J-PARC  $K^-$  exposure experiments as two-body  $\Xi^-$  capture in  ${}^{12}\text{C}$  and  ${}^{14}\text{N}$  into twin  $\Lambda$  hypernuclei correspond to capture from  $1p_{\Xi^-}$  Coulomb-assisted bound states. This involved using just one *common* strength parameter of a density dependent optical potential. Long-range  $\Xi N$  shell-model correlations were essential in making the  ${}^{14}\text{N}$  events consistent with the  ${}^{12}\text{C}$  events. Earlier attempts to explain these data overlooked this point, therefore

<sup>2</sup>Note that  $\text{Im } b_1=0$  because the charge exchange  $\Xi^- + {}^{11}\text{B} \rightarrow \Xi^0 + {}^{11}\text{Be}$  is kinematically blocked.

reaching quite different conclusions [50, 51, 52, 53, 54]. Predicted then are  $1s_{\Xi^-}$  bound states with  $B_{\Xi^-}^{1s} \sim 10$  MeV in  $^{12}\text{C}$  and somewhat larger in  $^{14}\text{N}$ , deeper by 4–5 MeV than the  $1s_{\Xi^-}$  states claimed by a recent J-PARC E07 report of multibody capture events [24]. The  $\Xi$  nuclear-matter potential depth derived here within an optical potential methodology,  $V_{\Xi} = 21.9 \pm 0.7$  MeV, is considerably larger than  $G$ -matrix values below 10 MeV derived from recent LQCD and EFT  $\Xi N$  potentials [27, 29]. A systematic optical-potential model uncertainty of less than 1 MeV as discussed in Sect. 5 is short of bridging the gap noted above. Substantial  $\Xi NN$  three-body *attractive* contributions to the  $\Xi$  nuclear potential depth would be required to bridge this gap. Intuitively one expects repulsive  $BNN$  three-body contributions for octet baryons  $B$ , e.g. Ref. [31], but in chiral EFT studies, focusing on decuplet- $B^*$  intermediate  $B^*NN$  and  $BN\Delta$  configurations, this has been proven so far only for  $B = \Lambda$  [55, 56].

To check the procedure practised in Sect. 5 for fitting  $V_{\Xi}$  to just one  $\Xi^-$ - $^{12}\text{C}$  bound state datum, we apply it to the  $1s_{\Lambda}$  binding energy in  $^{12}\text{C}$ ,  $B_{\Lambda}^{1s} = 11.69 \pm 0.12$  MeV [57]. The fitted strength  $b_0 = 0.866 \pm 0.010$  fm amounts to a nuclear-matter  $\Lambda$  potential depth  $V_{\Lambda} = 31.7 \pm 0.2$  MeV, in good agreement with the accepted value  $V_{\Lambda} \approx 30$  MeV [7]. One may slightly improve the derived value of  $V_{\Lambda}$  by subtracting from  $B_{\Lambda}^{1s}$  a nuclear induced spin-orbit contribution that vanishes in the limit  $A \rightarrow \infty$ , thereby reducing our input  $B_{\Lambda}^{1s}$  to 10.85 MeV [49]. This gives  $b_0 = 0.798 \pm 0.010$  fm and  $V_{\Lambda} = 30.5 \pm 0.2$  MeV. Here too it is not possible to separate the contribution of  $\Lambda NN$  three-body potential terms from that of the main  $\Lambda N$  two-body potential term.

A strong  $\Xi$ -nuclear interaction, such as derived here, may have far-reaching implications to  $(N, \Lambda, \Xi)$  strange hadronic matter [10] and particularly to dense neutron star matter [11]. In the latter case a strong  $\Xi$ -nuclear interaction might cause a faster depletion of  $\Lambda$  hyperons by  $\Lambda\Lambda \rightarrow \Xi^- p$ , a process inverse to the  $\Xi^-$  capture reaction considered in the present work. More work is necessary in this direction.

## Acknowledgments

Recent related correspondence with Johan Haidenbauer, Jiří Mareš, John Millener, Tomofumi Nagae, Josef Pochodzalla and Tom Rijken is gratefully acknowledged. The present work is part of a project funded by the European

Union's Horizon 2020 research & innovation programme, grant agreement 824093.

## References

- [1] S. Acharya, et al. (ALICE Collaboration), Phys. Rev. C 99 (2019) 024001.
- [2] S. Acharya, et al. (ALICE Collaboration), Phys. Lett. B 797 (2019) 134822.
- [3] S. Acharya, et al. (ALICE Collaboration), Phys. Rev. Lett. 123 (2019) 112002.
- [4] S. Acharya, et al. (ALICE Collaboration), Nature 588 (2020) 232.
- [5] K. Sasaki, et al. (HAL QCD Collaboration), Nucl. Phys. A 998 (2020) 121737.
- [6] L. Tolos, L. Fabbietti, Prog. Part. Nucl. Phys. 112 (2020) 103770.
- [7] A. Gal, E.V. Hungerford, D.J. Millener, Rev. Mod. Phys. 88 (2016) 035004.
- [8] E. Hiyama, K. Nakazawa, Annu. Rev. Nucl. Part. Sci. 68 (2018) 131.
- [9] C.B. Dover, A. Gal, Ann. Phys. 146 (1983) 309.
- [10] J. Schaffner-Bielich, A. Gal, Phys. Rev. C 62 (2000) 034311, and references cited therein to earlier work.
- [11] S. Weissenborn, D. Chatterjee, J. Schaffner-Bielich, Nucl. Phys. A 881 (2012) 62.
- [12] T. Fukuda, et al. (E224 Collaboration), Phys. Rev. C 58 (1998) 1306.
- [13] P. Khaustov, et al. (The AGS E885 Collaboration), Phys. Rev. C 61 (2000) 054603.
- [14] T. Harada, Y. Hirabayashi, Phys. Rev. C 103 (2021) 024605.
- [15] J.K. Ahn, et al., Phys. Rev. Lett. 87 (2001) 132504.

- [16] T. Nagae, et al., AIP Conf. Proc. 2130 (2019) 020015.
- [17] J. Pochodzalla, et al. (for the PANDA Collaboration), JPS Conf. Proc. 17 (2017) 091002.
- [18] C.Z. Yuan, M. Karliner, Phys. Rev. Lett. 127 (2021) 012003.
- [19] C.J. Batty, E. Friedman, A. Gal, Phys. Rev. C 59 (1999) 295.
- [20] D. Zhu, C.B. Dover, A. Gal, M. May, Phys. Rev. Lett. 67 (1991) 2268.
- [21] S. Aoki, et al. (KEK E176 Collaboration), Nucl. Phys. A 828 (2009) 191, and earlier E176 publications cited therein.
- [22] H. Nakazawa, et al. (KEK PS-E373), Prog. Theor. Exp. Phys. 2015 (2015) 033D02.
- [23] S.H. Hayakawa, et al. (J-PARC E07 Collaboration), Phys. Rev. Lett. 126 (2021) 062501.
- [24] M. Yoshimoto, et al. (J-PARC E07), Prog. Theor. Exp. Phys. 2021 (2021) 073D02.
- [25] T. Koike, JPS Conf. Proc. 17 (2017) 033011.
- [26] C.B. Dover, J. Hüfner, R.H. Lemmer, Ann. Phys. 66 (1971) 248.
- [27] T. Inoue (for HAL QCD Collaboration), AIP Conf. Proc. 2130 (2019) 020002.
- [28] J. Haidenbauer, U.-G. Meißner, Eur. Phys. J. A 55 (2019) 23.
- [29] M. Kohno, Phys. Rev. C 100 (2019) 024313.
- [30] T. Gaitanos, A. Choroizidou, Nucl. Phys. A 1008 (2021) 122153.
- [31] M.M. Nagels, Th.A. Rijken, Y. Yamamoto, Phys. Rev. C 102 (2020) 054003; see in particular Tables XXI, XXIV for models ESC16\*(A,B) respectively.
- [32] E. Friedman, A. Gal, Phys. Rep. 452 (2007) 89.
- [33] L.R.B. Elton, *Nuclear Sizes*, (Oxford Univ. Press, Oxford, 1961).

- [34] I. Angeli, K.P. Marinova, *At. Data Nucl. Data Tables* 99 (2013) 69.
- [35] C.W. de Jager, H. de Vries, C. de Vries, *At. Data Nucl. Data Tables* 14 (1974) 479.
- [36] H. de Vries, C.W. de Jager, C. de Vries, *At. Data Nucl. Data Tables* 36 (1987) 495.
- [37] A. Gal, E. Friedman, C.J. Batty, *Nucl. Phys. A* 606 (1996) 283.
- [38] S. Ajimura, et al., *Phys. Rev. Lett.* 86 (2001) 4255.
- [39] J. Mareš, B.K. Jennings, *Phys. Rev. C* 49 (1994) 2472.
- [40] E.H. Auerbach, A.J. Baltz, C.B. Dover, A. Gal, S.H. Kahana, L. Ludeking, D.J. Millener, *Phys. Rev. Lett.* 47 (1981) 1110, *Ann. Phys.* 148 (1983) 381 where values of  $-F_{\Lambda N}^{(2)} = 3.0 - 3.4$  MeV were proposed.
- [41] A. de-Shalit, I. Talmi, *Nuclear Shell Theory* (AP, New York, 1963).
- [42] R.H. Dalitz, A. Gal, *Ann. Phys.* 131 (1981) 314.
- [43] D.J. Millener, in *Topics in Strangeness Nuclear Physics*, Edited by P. Bydžovský, A. Gal, and J. Mareš, *Lecture Notes in Physics* 724 (Springer, Heidelberg, 2007) 31-79.
- [44] T. Waas, M. Rho, W. Weise, *Nucl. Phys. A* 617 (1997) 449.
- [45] E. Friedman, A. Gal, *Nucl. Phys. A* 899 (2013) 60, *Nucl. Phys. A* 959 (2017) 66.
- [46] W. Weise, R. Härtle, *Nucl. Phys. A* 804 (2008) 173.
- [47] E. Friedman, A. Gal, J. Mareš, *Phys. Lett. B* 725 (2013) 334.
- [48] A. Cieplý, E. Friedman, A. Gal, J. Mareš, *Nucl. Phys. A* 925 (2014) 126.
- [49] D.J. Millener, *Nucl. Phys. A* 881 (2012) 298.
- [50] M. Yamaguchi, K. Tominaga, Y. Yamamoto, T. Ueda, *Prog. Theor. Phys.* 105 (2001) 627.
- [51] E. Hiyama, Y. Yamamoto, H. Sagawa, *Phys. Scr.* 91 (2016) 093001.

- [52] T.T. Sun, E. Hiyama, H. Sagawa, H.-J. Schulze, J. Meng, Phys. Rev. C 94 (2016) 064319.
- [53] J. Hu, H. Shen, Phys. Rev. C 96 (2017) 054304.
- [54] Y. Jin, X.-R. Zhou, Y.-Y. Cheng, H.-J. Schulze, Eur. Phys. J. A 56 (2020) 135.
- [55] S. Petschauer, J. Haidenbauer, N. Kaiser, U.-G. Meißner, W. Weise, Nucl. Phys. A 957 (2017) 347.
- [56] D. Gerstung, N. Kaiser, W. Weise, Eur. Phys. J. A 56 (2020) 175.
- [57] D.H. Davis, Nucl. Phys. A 754 (2005) 3c.